



HHS Public Access

Author manuscript

Aging Biol. Author manuscript; available in PMC 2024 September 05.

Published in final edited form as:

Aging Biol. 2023 ; 1(1): . doi:10.59368/agingbio.20230014.

Cellular senescence exacerbates features of aging in the eyes

Koji Kitazawa^{1,2,*}, Kohsaku Numa^{1,2}, Sandip Kumar Patel¹, Christina D. King¹, Akifumi Matsumoto², Chie Sotozono², Pierre-Yves Desprez¹, Birgit Schilling¹, Judith Campisi^{1,*}

¹Buck Institute for Research on Aging, 8001 Redwood Boulevard, Novato, CA 94945, USA;

²Kyoto Prefectural University of Medicine, Department of Ophthalmology, Kyoto, 6020841, Japan;

Abstract

Aging is a process often associated with various age-related diseases. Senescence is one of the hallmarks of aging, and senescent cells acquire a complex, often pro-inflammatory, secretory phenotype termed the senescence-associated secretory phenotype (SASP). Here we show that ocular surface cells from human cornea become senescent upon X-irradiation, characterized by increased SA- β -gal activity, decreased cell proliferation, increased expression of p16, and disruption of epithelial barrier. Comprehensive transcriptomic and proteomic analysis revealed that human senescent ocular cells acquire a SASP that disrupts epithelial barrier function. During aging in mice, senescent ocular cells accumulate, resulting in decreased epithelial barrier and chronic inflammation. Lacrimal gland excision, which leads to symptoms of dry eye (DE), resulted in corneal opacity associated with severe angiogenesis only in aged mice but not in young mice, and early senolytic treatment protected old DE mice from corneal opacity. In conclusion, senescent cells alter the ocular microenvironment through their SASP and eliminating these cells could represent a potential approach to alleviate symptoms associated with aged ocular surface.

Keywords

senescence-associated secretory phenotype; mouse models; lacrimal gland excision; ocular surface; proteomics; dry eye

INTRODUCTION

The aging population is rapidly increasing throughout the world. Aging is an universal process that affects numerous pathological conditions for age-related eye diseases, such as dry eye (DE), cataract, glaucoma and macular degeneration. We previously investigated the ocular surface changes during aging in humans and mice¹, and observed some

*Correspondence: Koji Kitazawa, Kyoto Prefectural University of Medicine, Department of Ophthalmology, Kyoto, 6020841, Japan; Fax: +81-75-251-5579, kkitazaw@koto.kpu-m.ac.jp; Judith Campisi, Buck Institute for Research on Aging, 8001 Redwood Boulevard, Novato, CA 94945, USA; Fax: 1-415-493-3640, jcampisi@buckinstitute.org.

AUTHOR CONTRIBUTIONS

KK, PYD, BS, JC designed the experiments; KK, KN, SKP, CDK, AM conducted the experiments; KK, PYD, BS, JC analyzed the data; KK, SKP, AM, CS, PYD, BS, JC wrote or edited the manuscript.

COMPETING FINANCIAL INTERESTS

The authors declare no competing financial interests. JC is a founder of Unity Biotechnology, which develops methods to eliminate senescent cells.

senescence-like chronic inflammation, including accumulation of 8-OHdG and lipofuscin-like inclusions, increased expression of p53 and apoptosis-related genes, and decreased Ki67-positive cells^{2–6}. However, it was not clear how this chronic inflammation could influence the aged ocular surface, and the causes of this inflammation had yet to be determined.

Hallmarks of aging include genomic instability, telomere attrition, epigenetic alterations, loss of proteostasis, dysregulated nutrient sensing, mitochondrial dysfunction, cellular senescence, stem cell exhaustion, and altered intercellular communication⁷. These age-related changes drive non-pathogenic and chronic low-grade inflammation, which is primarily caused by senescent and immune cells⁸. Cellular senescence is one of the hallmarks of aging and is a cell fate in which both intrinsic and extrinsic signals cause an irreversible cell cycle arrest^{9,10}, accompanied by many phenotypic changes such as enlarged cell morphology, chromatin reorganization, altered gene expression, and increased glycolytic metabolism and production of reactive oxygen species¹¹. Furthermore, senescent cells acquire a complex, often pro-inflammatory, secretory phenotype termed the SASP. Among the molecules often secreted by senescent cells are pro-inflammatory cytokines (e.g., IL-6, IL-8 and IL-1b), chemokines (e.g., CXCL5 and CXCL10) and MMPs (e.g., MMP1, MMP3 and MMP9)^{12,13}. These molecules are frequently associated with a variety of age-associated pathologies, including many that are characterized by chronic inflammation^{14–16}. Ocular surface inflammation promotes conjunctival squamous metaplasia¹⁷ and inflammation-associated barrier dysfunction¹⁸, resulting in the development of refractory corneal diseases. However, the causes of inflammation at the ocular surface and how the ocular surface is altered during aging are still to be determined.

In the present study, we established cell culture and mouse models to examine the phenotype of human senescent ocular cells (SOC), and the role of senescent cells in aged ocular surface *in vivo*. We show that accumulation of cellular senescence at the ocular surface is associated with chronic inflammation and disruption of the epithelial barrier, leading to refractory ocular surface diseases, including corneal opacity, associated with severe angiogenesis.

MATERIALS AND METHODS

Cell cultures and treatments

We used primary CoC isolated from human donor corneas (CorneaGen, Seattle Eye Bank, WA). CoC were isolated and cultured as previously described¹⁹ with minor modifications. Corneas and conjunctivas were treated with Dispase type II (Godo Shusei, Tokyo, Japan) at a concentration of 1000 PU/ml at 4°C overnight, and corneal/conjunctival epithelium was peeled off. CoC were then dissociated using TrypLE™ Express (Thermo Fisher Scientific, Waltham, MA) for 5 min at 37°C and seeded onto single wells of 6-well plates. CoC were cultured at 37°C at 95% humidity and 5% CO₂ in complete CEC medium²⁰, consisting of Dulbecco's modified Eagle's and Ham's F-12 media (DMEM/F12, 1:1 mixture) (Thermo Fisher Scientific), B-27™ supplement (2%) (Thermo Fisher Scientific), Rho-kinase inhibitor Y-27632 (10 μM) (Selleck Chemicals, Houston, TX), keratinocyte growth factor (10 ng/ml) (Thermo Fisher Scientific), and penicillin-streptomycin (50 IU/ml) (Nacalai Tesque).

Cultured CoC were used for subsequent experiments after one passage using TrypLE™ Express (Thermo Fisher Scientific) at room temperature upon reaching sub-confluence.

We generated SOC from primary human corneal and conjunctival cells using IR (10 Gy) or the chemotherapeutic agent DOXO (250 nM for 24 h), which intercalates into DNA and disrupts topoisomerase-II-mediated DNA repair^{21,22}. SOC were cultured for 10 days to allow the development of a full senescent phenotype. Mock-treated cells or cells treated with DMSO were used as controls.

SA-β-gal staining and EdU labeling

Cells were fixed and processed for SA-β-gal staining as per the manufacturer's instruction (Biovision, Waltham, MA). A Nikon Eclipse E800 microscope was used for imaging, and images were quantified using Image J software. Cell proliferation was evaluated by incorporation of EdU and the Click-iT EdU Cell Proliferation Assay Kit (Invitrogen). Briefly, cells were given 10 μM EdU for 24 h before fixation, permeabilized and incubated with Click-iT reaction cocktail as per the manufacturer's instruction. A microscope (Nikon Eclipse E800) was used for imaging, and images were quantified using Image J software. >100 cells from 5 different fields were quantified per condition, and all experiments were done in triplicate.

qRT-PCR analysis

RNA was isolated from cultured cells and homogenized tissues using the Bioline Isolate II RNAMini Kit (Meridian Bioscience, Cincinnati, OH) as recommended by the supplier. Complementary DNA was synthesized from 500–1000 ng of total RNA using High-Capacity cDNA Reverse Transcription Kit (Thermo Fisher Scientific). qRT-PCR was performed using the LightCycler® 480 Real-Time PCR System (Roche Applied Science, Penzberg, Germany) as described previously²³. The $2^{-\Delta\Delta Ct}$ method was used to calculate expression levels normalized to human or mouse ACTB Endogenous Control (Thermo Fisher Scientific). All the primers used for the experiments are listed in Tables S6 and S7.

Conditioned media

Irradiated corneal epithelial cells (SOC) or non-senescent mock cells (NS) were cultured in complete media, washed three times with PBS and placed in DMEM/F12 (serum- and supplement-free media) (Thermo Fisher Scientific) for 2 days. Subsequently, cells were washed with PBS and placed in phenol red-free DMEM/F12, and CM were collected after 24 h. A total of 150,000 cell equivalents/ml of CM was used for barrier function assays. Collected CM were also used for mass spectrometry analysis.

Cell viability assay upon ABT263 treatment

To determine the dose of ABT263 (Selleck Chemicals, Houston, TX) that specifically kills SOC and not NS cells, cell viability was assessed using the cell counting kit-8 (Dojindo Molecular Technologies, Inc, Rockville, MD). SOC or NS were incubated in complete media plus 10% cell viability kit reagent, 150 μl/well in 96-well plates for 2 h at 37°C. Supernatants were transferred to new 96-well plates and absorbance read at 450 nm. For the subsequent culture experiments, fresh complete media containing or not ABT263 were used.

Immunofluorescence staining

Fresh tissues from normal mouse corneas were embedded in Tissue-Tek OCT, cryopreserved, and sectioned (7 μm). Immunostaining of corneal sections was performed according to a previously reported method²⁴ with modifications. Briefly, cryosections were incubated at room temperature for 1 min and then fixed with 4% PFA at 4°C for 10 min. After aspiration of the fixative, sections were rinsed with PBS for 5 min and permeabilized with 0.05% Triton-X-100 at room temperature for 30 min. Samples were blocked with 10% goat serum at room temperature for 45 min and then incubated with F4/80 primary antibody (Abcam, #ab6640, 1:200 dilution) overnight at 4 °C. The next day, samples were washed with PBS and incubated with a secondary antibody (Invitrogen, Alexa Fluor 594-conjugated anti-rat IgG) at a dilution of 1:1000 for 1 h at room temperature. After washing, DAPI was added. Sections were viewed using a fluorescence microscope (Nikon Eclipse E800) and photographed.

Western blotting

Cells were washed with ice-cold PBS and lysed with RIPA buffer supplemented with 2-mercaptoethanol (final concentration 6%) and Halt Protease and Phosphatase Inhibitor Cocktail (Thermo Fisher Scientific), then boiled for 5min at 95°C. Equal amounts (10–30 μg) of samples were loaded and proteins were separated by SDS-PAGE using 4–12 % Bis-Tris gels (Bio-Rad, Hercules, CA), followed by transfer to PVD membranes using iBlot Dry Blotting Gel Transfer System (Thermo Fisher Scientific). Membranes were blocked for 1 h in 5% BSA-TBST or 5% milk-TBST at room temperature, and then incubated with primary antibodies overnight at 4°C. Blots were washed and incubated with HRP-conjugated secondary antibodies for 1 h at room temperature, and detection was performed using enhanced chemiluminescence. Primary antibodies were against p16 (Abcam, #ab108349, 1:500 dilution) and HMGB1 (Abcam, #ab18256, 1:500 dilution). Secondary antibodies were HRP-conjugated goat anti-rabbit (Bio-Rad) and goat anti-mouse (Bio-Rad) antibodies. An antibody against beta actin (Sigma, #A2228, 1:10,000 dilution) was used for loading control.

Barrier function in culture

To measure barrier function of ocular surface cells, we used a volt-ohm meter (EVOM, World Precision Instruments) as we previously reported²⁵. Non-senescent CoC (NS) or SOCs cultured with NS at a ratio of 75% to 25% were seeded at a cell density of 100,000 cells per well in 24-well transwell plates (Corning, 24-mm Transwell with 0.4- μm Pore Polyester Membrane Insert). Upon reaching 100% confluence, cells were tested for TEER between the upper and lower chambers of permeable cell culture inserts using the volt-ohm meter. The TEER was measured and calculated by multiplying the measured resistance (ohms) by the growth area of the transwell filter. The background resistance due to the filter alone was subtracted from each of the measurements. The TEER was measured twice and the average value was used for analysis.

Next generation RNA-Seq

An initial quality assessment of raw RNA-seq data was performed using FastQC (v0.12.1; <https://www.bioinformatics.babraham.ac.uk/projects/fastqc/>) to evaluate read quality.

TrimGalore (v4.3; https://www.bioinformatics.babraham.ac.uk/projects/trim_galore/)²⁶ was conducted to remove adapter sequences, and low-quality reads. The trimmed reads were aligned to the reference genome (GRCh38) using HISAT2 (v2.2.1)²⁷. We converted the output SAM files to sorted BAM files with SAMtools (v1.12)²⁸ for downstream analysis. FeatureCounts (v2.0.3)²⁹ was utilized to assign mapped reads to their corresponding genes, generating count data for each gene. The raw read counts were normalized using DESeq2 (v1.8.3)³⁰. We performed differential gene expression analysis with DESeq2 (v1.8.3) in R (v4.2.3; <https://www.R-project.org/>) and RStudio (v2023.03.0+386; <https://www.rstudio.com/>). Gene ontology (GO) and pathway analysis for the identified differentially expressed genes (DEGs) were carried out using the clusterProfiler (v4.6.2) package.

Isolation of corneal SASP proteins

A detailed list of reagents and resources used in the proteomics analysis, including vendors and catalog numbers, is available in the Reagent and Resource Table (Table S8). Briefly, protein sample processing was performed as follows. Conditioned media from corneal cells (quiescent control and IR-treated cells [n = 3 each]) were collected as previously described¹³. Salt and other media components were removed using 3 kDa cutoff columns (Amicon Centrifugal Filters), and SASP protein extracts were subsequently lysed using lysis buffer (5% SDS and 50 mM TEAB). Each extract was reduced by incubation with 20 mM dithiothreitol in 50 mM TEAB for 10 min at 50°C, and subsequently alkylated with 40 mM iodoacetamide in 50 mM TEAB for 30 min at RT in the dark. Extracts were acidified to yield pH < 1 using phosphoric acid (v/v) and subsequently 100 mM TEAB in 90% methanol were added.

The entire protein extracts were spun through the micro S-Trap columns (Protifi). Subsequently, the S-Trap columns were washed with 90% methanol in 100 mM TEAB, placed in clean elution tubes and incubated with trypsin digestion buffer (50 mM TEAB, pH ~8) at a 1:25 ratio (protease:protein, wt:wt) overnight. Peptides were then sequentially eluted with 50 mM TEAB and 0.5% formic acid, and 50% acetonitrile in 0.5% formic acid. Both fractions were pooled together, vacuum dried and re-suspended in 0.2% formic acid for desalting. The desalted peptides were concentrated and re-suspended in aqueous 0.2% formic acid for mass spectrometry-based quantitative analysis.

Mass spectrometric data-independent acquisition (DIA)

Eight microliters of each sample were diluted with 2% acetonitrile (ACN) in 0.1% formic acid to obtain a concentration of 400 ng/ μ L. One microliter of indexed Retention Time Standard (iRT, Biognosys, Schlieren, Switzerland) was added to each sample as internal standard, thus bringing up the total volume to 20 μ L³¹. Reverse-phase HPLC-MS/MS analyses were performed on a Dionex UltiMate 3000 system coupled online to an Orbitrap Exploris 480 mass spectrometer (Thermo Fisher Scientific, Bremen, Germany). The solvent system consisted of 2% ACN, 0.1% Formic acid (FA) in water (solvent A) and 80% ACN, 0.1% FA in ACN (solvent B).

Digested peptides (400 ng) were loaded onto an Acclaim PepMap 100 C₁₈ trap column (0.1 × 20 mm, 5 μm particle size; Thermo Fisher Scientific) over 5 min at 5 μl/min with 100% solvent A. Peptides (400 ng) were eluted on an Acclaim PepMap 100 C₁₈ analytical column (75 μm × 50 cm, 3 μm particle size; Thermo Fisher Scientific) at 300 nl/min using the following gradient: linear from 2.5% to 24.5% of solvent B in 125 min, linear from 24.5% to 39.2% of solvent B in 40 min, up to 98% of solvent B in 1 min, and back to 2.5% of solvent B in 1 min. The column was re-equilibrated for 30 min with 2.5% of solvent B, and the total gradient length was 210 min. Each sample was acquired in DIA mode^{32–34}. Survey MS1 spectra were collected at 120,000 resolution (AGC target: 3e6 ions, maximum injection time: 60 ms, 350–1,650 *m/z*), and MS2 spectra at 30,000 resolutions (AGC target: 3e6 ions, maximum injection time: Auto, Normalized Collision Energy (NCE): 30, fixed first mass 200 *m/z*). The isolation scheme consisted of 26 variable windows covering the 350–1,650 *m/z* range with a window overlap of 1 *m/z*³³.

DIA data processing and statistical analysis

DIA data was processed in Spectronaut v15 (version 15.1.210713.50606; Biognosys) using directDIA. Data was searched against the *homo sapiens* proteome with 42,789 protein entries (UniProtKB-TrEMBL), accessed on 12/07/2021. Trypsin/P was set as digestion enzyme and two missed cleavages were allowed. Cysteine carbamidomethylation was set as fixed modification, and methionine oxidation and protein N-terminus acetylation as variable modifications. Data extraction parameters were set as dynamic. Identification was performed using 1% precursor and protein q-value (experiment). Quantification was based on MS2 area, local normalization was applied, and iRT profiling was selected. Differential protein expression analysis was performed using a paired t-test, and q-values were corrected for multiple testing, specifically applying group wise testing corrections using the Storey method³⁵. Protein groups with at least two unique peptides, q-value < 0.05, and absolute Log₂ (fold-change) > 0.58 were considered to be significantly altered, and are listed in Table S2.

Animals

Animal studies were conducted in compliance with protocols approved by the IACUC of the Buck Institute for Research on Aging. Animals were maintained in a controlled environment (20–22°C; 12 h light:12 h dark cycle). We engineered a bacterial artificial chromosome in which the p16 promoter drives the expression of a fusion protein (3MR) containing rLUC, RFP and a HSV-TK. RFP enables the sorting of 3MR-expressing cells from tissues. HSV-TK enables the elimination of 3MR-expressing cells using GCV, a nucleoside analogue that has a high affinity for HSV-TK, but low affinity for cellular TK, and is converted into a toxic moiety by the HSV-TK^{36–38}. C57BL/6 mice or p16-3MR mice were used in this study. To eliminate senescent cells in p16-3MR homozygous female mice, 0.3% topical GCV treatment was performed, whereas topical PBS treatment was used as control.

Lacrimal gland excision

Animals were placed under general anesthesia using 3% isoflurane. Incisions anterior to the ear to expose the external lacrimal gland were performed. Lacrimal glands were excised from the orbit using ophthalmic forceps with the aid of a stereoscopic microscope. Gland

excisions were performed on both right and left sides. After surgery, mice were evaluated for corneal surface integrity after application of fluorescein, and tear production was assessed as described below.

Tear volume and corneal fluorescein staining *in vivo*

The tear storage volume of each eye was measured twice with phenol-red impregnated cotton threads (Zone-Quick; FCI Ophthalmics), and was averaged as an index of the tear retaining action. The cotton thread was placed on the ear conjunctiva of the mouse and the amount of the tears was measured for 15 seconds, followed by immediately measuring the length of the wet portion of the thread. To evaluate the barrier function of the corneal epithelium, corneal epithelial damage was assessed with fluorescein staining under the handy slit lamp with blue filter illumination (XL-1; Reexam). A corneal fluorescein staining score was assigned at each 1/3 area of the cornea (upper, intermediate, and lower). The score was categorized from 0 to 3 (0 = no fluorescence, 1 = fluorescence evident as sparse dots, 2 = dense dot-like fluorescence pattern, 3 = very dense dot-like fluorescence) assessed by an unbiased observer, as previously reported³⁹.

Statistics

All data with error bars are presented as mean \pm S.E.M, and the individual data points (dots) are presented in the bar graphs. Statistical analyses were performed using Prism 9 software with 9.2.0 (283) (GraphPad, La Jolla, CA, USA). Comparisons between groups were conducted with one-way analysis of variance (ANOVA), followed by the post hoc Dunnett's multiple comparison test. Welch's adjusted t-test (also called unequal variances t-test), a modified Student's t-test, was also used under the assumption of unequal variances. Most of cell culture experiments were done in triplicate and reproduced at least three times independently.

RESULTS

Role of human senescent ocular cells (SOCs) in the inflammatory phenotype at the ocular surface

The ocular surface is composed of cornea, conjunctiva, and tear fluid. Accumulation of senescent cells during aging is part of the hallmarks of aging. In order to characterize the features of SOC, we induced cellular senescence in human primary corneal epithelial cells upon treatment with a DNA damaging agent, ionizing radiation. Irradiated human SOCs showed higher SA- β -Gal staining and lower incorporation of EdU than non-irradiated cells, indicating cellular senescence induction (Fig. 1a). Irradiated human SOCs secreted pro-inflammatory factors that are part of the SASP, which are also expressed by several types of senescent cells. These factors included *IL-6*, *IL-1 β* , *MMP-3*, *MMP-9* and *TNF- α* , in addition to the expected upregulation of the cell cycle inhibitors *p16^{INK4a}* (p16) and *p21^{WAF1/Cip1}* (p21), and down-regulation of the nuclear protein *LMNB1* and HMGB1, at mRNA levels (Fig. 1b, d) and protein levels (Fig. 1c), as we previously reported in other cell types undergoing senescence^{12,40–42}. These data show that human ocular cells undergoing DNA damage acquire a SASP, which could potentially be causal to the inflammation detected at ocular surfaces during aging.

Disruption of the corneal epithelial barrier by SOC

The ocular surface evolved to protect the cornea, and keep it smooth and wet, a prerequisite for proper eyesight. With age, the ocular surface becomes more vulnerable to external stimuli⁴³, as is the case for many other tissues. In order to examine the effects of SOC on epithelial barrier function, the transepithelial electrical resistance (TEER) was measured. SOC were co-cultured with control NS at a ratio of 75 to 25, and cells being fully confluent in culture inserts. SOC appeared larger than NS (Fig. 2a), and TEER readings in co-cultures were lower compared to NS cultures (Fig. 2b). Next, we determined whether the decrease in TEER was due to SOC themselves or to the SASP they secrete. CM from SOC, which contained the SASP, were collected and added to NS to determine whether the TEER would be modified. CM collected 3 days after senescence induction triggered a significant decrease in TEER readings (Fig. 2c), suggesting that some SASP factors disrupt the corneal epithelial barrier, which is a key component of ocular surface.

To confirm that senescent cells are responsible for the disruption of barrier function, we tested whether the decreased in TEER was reversed upon removal of senescent cells with a senolytic drug, ABT263. ABT263 is a Bcl-inhibitor and started to kill SOC selectively three days after the initiation of treatment. Cell viability of SOC was decreased by 70% compared to NS at 0.1 μM of ABT263 on day 7 of the treatment (Fig. 2d). The improvement in TEER was consistent with the effect of ABT263 on SOC over time and, on day 7, the values reached levels close to control NS (Fig. 2e). Overall, our data suggest that SOC contribute to the disruption of the corneal epithelial barrier through the secretion of SASP factors. We determined that, not only inflammatory cytokines, but also chemokines-related genes such as *CCL2*, *CXCL3*, *CXCL8*, *CXCL9*, and *CXCL10*, were highly expressed by SOC compared to NS (Fig. 2f).

Next, we analyzed the global gene expression profile of SOC using RNA-seq as an unbiased approach. Global differential expression analyses between SOC and NS revealed 3,234 significantly differentially expressed genes, with $|\log\text{FC}| > 1.0$ and adjusted p-value < 0.05 (Fig. 2g and Table S1). Comparison of SOC and NS showed that a high proportion of the differentially expressed genes, i.e., 2,102 genes were upregulated and 1,132 genes were downregulated in SOC. Downregulated genes are significantly associated with enriched gene ontology (GO) terms related to organelle fission, nuclear division, DNA replication, and mitotic cell cycle phase transition (Fig. 2h and Table S2a), which are all modulated during cellular senescence. Upregulated genes are significantly associated with enriched GO terms related to positive regulation of leukocyte migration and chemotaxis, and extracellular structure organization (Fig. 2i and Table S2b), suggesting that SOC acquires an inflammatory phenotype. Moreover, matrix metalloproteinase genes, such as *MMP8*, *MMP12*, *MMP7*, *MMP24*, *MMP15*, *MMP10*, *MMP3*, and *MMP1*, were upregulated, which could explain the disruption of the corneal epithelial barrier (Fig. 2b–c).

Characterization of the SASP components secreted by SOC

The SASP exhibits multifunctional aspects and depends on the cell types¹³, physiological states⁴⁰, and environmental stimuli⁴⁴. We therefore analyzed the SASP factors secreted by SOC using a label-free, unbiased quantitative mass spectrometric approach, referred to as

data-independent acquisition (DIA)³⁴. The proteomics analysis of conditioned media from human SOC and mock revealed 636 quantifiable proteins (2 unique peptides) (Table S3a). Partial least squares-discriminant analysis (PLS-DA) clustered IR-induced senescence and mock corneal SASP, and 91% variate contributed to this conclusion (Fig. S1a–b). Out of 639 quantifiable corneal SASP proteins, 609 proteins were significantly altered in senescence compared to mock (fold change 1.5, q-value 0.05) as shown in Table S3b and Fig. 3a, of which 429 proteins showed strong secretion, and 180 proteins were decreased as presented in the volcano plots. Further, to emphasize the heterogeneity of the SASP profiles in different cell types, we compared the corneal epithelial SASP with the IR-induced SASP from human lung fibroblasts (IMR90 cells) as shown previously¹³. We determined that 427 and 367 SASP proteins were unique to epithelial cells and fibroblasts, respectively (Fig. 3b), while 179 SASP proteins overlapped (Fig. 3b and Table S3). Based on the present analysis, GDF15, MMPs, and SERPIN proteins are integral to SASP from both epithelial cells and fibroblasts (Table S4) as we previously reported¹³, suggesting that multiple senescent cell types exhibit some important and common SASP factors.

The top 10 corneal SASP proteins showing increased and limited secretions are presented in Fig. 3c and Table S2b, and some of the most promising candidate factors for the biological effects of SOC, which include GDF15, CAPS, LUM, and LTBP3, are displayed in Fig. 3d. GDF15 belongs to the TGF- β superfamily proteins, which are highly expressed in human aged corneas⁴⁵. We found that GDF15 was upregulated in SOC both at RNA levels (Fig. 3e and Table S1b) and at secreted protein levels (Fig. 3f). Calcyphosin is a calcium/metal-binding protein increased during cellular senescence⁴⁶, LUM is a keratan sulfate proteoglycan of the small leucine rich proteoglycan family originally identified in cornea, and LTBP3 is a key regulator of TGF- β 1, - β 2, and - β 3.

Functional analysis using GO term revealed that ubiquitin-dependent degradation of cyclin D1, p53-independent DNA damage response, and G1/S DNA damage checkpoint pathways associated with senescence-induction were up-regulated (Fig. 3g, Fig. S2, and Table S5a). Up-regulation of the immune system and interleukin signaling suggests a role of the SASP in the inflammation at the ocular surface, possibly via inflammatory cell infiltration within ocular tissue (Fig. 3g and Fig. S2). Moreover, up-regulation in metalloaminopeptidase activity and keratinization related proteins (Fig. 3g and Fig. S2), and down-regulation of axon- and neuron projection-regeneration, could be associated with loss of biological function in SOC (Fig. 3g–h, Fig. S3, and Table S5b). Interestingly, down-regulation of cell junction assembly could lead to the disruption of barrier function in corneal epithelial cells, a function that is vital for a healthy eye (Fig. 3h).

Comparison of ocular surfaces using a DE model in young and old mice

We investigated the potential link between the presence of senescent cells and an age-related ocular surface disease (dry eye, DE). We determined that the tear fluid volume was higher in old mice than in young mice (Fig. 4a), unlike humans as previously reported^{47,48}. Thus, we created a mouse model of severe DE in young mice (4 months of age) and old mice (24 months of age) (Fig. 4b). Extraorbital lacrimal gland excision (LGE) provides a simple and consistent model of severe aqueous tear-deficient DE. LGE results in tear film instability,

which, importantly, plays a central role to all forms of DE^{39,49–52}. Tear fluid secretion was measured after LGE and we determined that tear fluid volume was significantly lower in the LGE-treated eyes compared to sham eyes in both young and old mice (Fig. 4c). The anterior segment photographs show that transparency was maintained in young eyes. However, LGE-treated eyes in old mice displayed corneal opacity with severe angiogenesis (Fig. 4d). In addition to corneal opacity associated with angiogenesis, 60% of LGE-treated eyes displayed corneal keratinization (Fig. 4d).

We found that SOC in cell cultures could impair the epithelial barrier function and secreted various cytokines and chemokines. In order to investigate the potential role of cellular senescence in aged ocular surface, we compared the ocular surfaces in young mice (4 months of age) and old mice (24 months of age). We found that the expression of both p16 and p21 was significantly elevated in the cornea of old mice (Fig. 4e). In addition, we detected more punctate epithelial damage in the cornea of old mice compared to young mice (Fig. 4f–g), indicating that the epithelial barrier at the ocular surface is disrupted in old mice. We also found that SASP-related genes, including *Il-6*, *Il-1 β* , *Mmp3*, and *Tnf- α* as well as chemokines-related genes, such as *CCL2*, *CXCL3*, *CXCL9*, and *CXCL10*, were elevated in cornea of old mice compared to young mice (Fig. 4h–i), suggesting that the SASP secreted by SOC could be responsible for corneal opacity associated with severe angiogenesis in LGE-treated old mice. Interestingly, LGE in young mice did not trigger increased expression of *Cd68* as observed in old mice (Fig. 4j), suggesting that the presence of senescent cells is an important factor for the inflammatory phenotypes observed in old mice.

We next examined whether the ocular surface could become opaque at an old age when LGE was performed at a young age (Fig. 4k). Eyes that underwent LGE-treatment eventually showed corneal opacity, while none of the control eyes (no LGE-treatment) displayed corneal opacity during the time frame investigated (Fig. 4l). Histological analysis revealed that corneas post-LGE displayed a keratinized epithelium associated with an increased number of inflammatory cells (Fig. 4m), suggesting that senescent cells exacerbate ocular surface abnormalities during severe DE in aged eyes.

Partial reversibility of angiogenesis upon delayed elimination of p16-positive senescent cells

In order to determine the levels of involvement of senescence cells in corneal opacity during severe DE due to LGE, we attempted to selectively remove senescence cells in old mice using a senolytic approach. We previously reported that our p16-3MR mice allow the selective ablation of p16-positive-senescent cells upon treatment with ganciclovir (GCV), a nucleoside analogue that has a high affinity for HSV-TK but low affinity for cellular TK, and is converted into a toxic moiety by the HSV-TK^{14,36}. Although it is possible to administer GCV systemically, we used topical administration to mimic clinical applications, and determined the therapeutic benefits of eliminating senescent cells upon topical GCV treatment. First, we assessed the effect of 0.3% GCV eye drops for 2 weeks in old mice and we found that the senescent markers, *p16* and *p21*, as well as the SASP-related genes, *Mmp9* and *Vegf*, were significantly downregulated compared to PBS treatment (Fig. 5a).

Next, we examined topical GCV treatment in our experimental DE model. 0.3% GCV eye drops were administered one month after LGE, three times a day for 5-days for two cycles with a 2-day interval between the cycles (Fig. 5b). LGE in old mice drove corneal opacity associated with severe angiogenesis (Fig. 5c), and the severity of angiogenesis was partially reduced upon GCV treatment compared to control PBS treatment. Reversal of corneal opacity was also observed upon GCV treatment, whereas PBS-treated eyes worsened as epithelial cell hyperproliferation was observed at the peripheral cornea (Fig. 5c). We also determined that gene expression levels of *p16* and some SASP-related genes, *Il-6*, *Il-1 β* , *Mmp9* and *Vegf*, were elevated in control-treated LGE mice, but significantly downregulated upon topical GCV treatment in LGE mice (Fig. 5d). Since SOC secrete a variety of chemokines, we examined the expression of *Cd68* and *F4/80* within the ocular surface after LGE. We found these genes elevated in LGE-treated control eyes, but downregulated upon topical GCV treatment (Fig. 5e), as what was observed for the expression of SASP-related genes.

Early senolytic treatment protects from corneal opacity in old DE mice

Topical GCV treatment showed partial improvement in eye condition, but the transparency of the cornea was not completely reversed and the corneal opacity remained, which could be due to treatment timing. Therefore, we next tested whether a lower senescence burden triggered by early treatment with topical GCV could prevent corneal opacity and angiogenesis after LGE. Topical GCV treatment was administered starting one week before and finishing one week after LGE (Fig. 5f). All LGE-treated eyes became opaque when topical control PBS eye drops were added, while LGE-treated eyes were protected from corneal opacity and angiogenesis when topical GCV eye drops were added (Fig. 5g). Finally, two other cases displayed corneal opacity but a reduction in angiogenesis upon treatment with topical GCV. The decrease in senescence burden was associated with a decrease in expression of SASP-related genes and cytokines (Fig. 5h). The number of macrophages expressing *Cd68* and *F4/80* was also reduced upon treatment with topical GCV (Fig. 5i), indicating that elimination of SOC can change the microenvironment at the ocular surface, resulting in the protection from corneal opacity and angiogenesis in DE models of aged mice. These findings suggest that reducing the number of SOC at the ocular surface can prevent, or at least reduce, some features of severe DE induced by LGE in old mice.

DISCUSSION

The prevalence of various diseases increases exponentially with aging because of the accumulation of senescent cells^{53,54}. So far, there was no report on the ability of ocular surface cells to undergo senescence and on the features of their SASP as a cause of inflammation at the ocular surface. Here, we show that the aging process at the ocular surface is accompanied by an increase in senescence burden, and that a senolytic approach protected mice eyes from corneal opacity and angiogenesis in DE models in response to lacrimal gland excision.

One of the biological functions of SOC is the disruption of epithelial barrier function. Studies using human corneas have shown that this function decreases during aging^{43,55}.

Even though p53 expression has not been described in the cornea, it was reported that the expression of the senescent-associated markers p16^{INK4a} and p21^{CIP1} increased with age in the corneal epithelium of human donors⁴⁵. Similarly, in mouse studies, the barrier function declines, and corneal epithelial damage and corneal permeability increase with age^{6,18,48}. We investigated the role of cellular senescence using human cell cultures and *in vivo* mouse models, and we show that the disruption of the epithelial barrier function is a consequence of increased expression p16^{INK4a}, p21^{CIP1} and the SASP, ultimately driving impaired ocular surface and signs of DE. We therefore report here an important role for senescent cells at the ocular surface, particularly their ability to alter the microenvironment and their role in the appearance of corneal diseases.

Further, mass spectrometry analysis of conditioned media from SOC identified an increase of GDF15 and lower levels of LTBP3 in the senescent corneal SASP, which could lead to the activation of TGF- β . TGF- β 1 activates NF- κ B, resulting in a secondary cellular senescence⁴⁵ that exacerbates the inflammatory response. The matrix metalloproteinases identified play an important role in the maintenance of epithelial barrier function, suggesting that they could represent potential biomarkers indicating the decline of ocular surface function during aging. Mass spectrometry analysis also revealed an increase in keratinization and a decrease of neural phenotype. We previously reported that human primary corneal epithelial cells genetically depleted of PAX6, a master regulator of development and differentiation of eyes and neurons, underwent an upregulation of skin keratinocyte-related genes²⁴. Here, we report that SOC gain abnormal behavior compared to non-senescent cells, which could explain the loss of their biological functions.

Another important role of SOC is chronic inflammation due to a SASP generated upon accumulation of senescent cells during aging, driving several age-related diseases and being linked to many pathological hallmarks of aging⁵⁶. We show that corneas started to become opaque one week after LGE and, when elimination of senescent cells was performed after a month, it still resulted in irreversible scarring of the cornea. However, a treatment using senolytics one week earlier could maintain the cornea transparent even after LGE, suggesting that the prophylactic administration reduces the deleterious effects of senescent cells at the ocular surface, increases the barrier function and counterbalances the deleterious effects of the ocular SASP, resulting in the maintenance of healthy ocular surface.

The ocular SASP may explain the link between senescent cells and corneal opacity or angiogenesis. Senescent corneal epithelial cells have been detected at the surface layer of human corneal epithelium⁴⁵, and we have also previously reported the presence of p16-positive cells at the surface of human conjunctival epithelium, associated with a decrease in barrier function⁵⁷. Therefore, as shown in old mice, senescent corneal cells could lead to a decline in barrier function and result in epithelial damage. If there is enough tear fluid in old mice, transparency of the cornea is maintained even though corneal epithelial damage occurs due to DE. However, when the lacrimal gland is removed in old mice, SASP proteins in tear fluid, including GDF15, MMP, and VEGF, become concentrated under DE conditions, resulting in stronger ocular phenotypes characterized by corneal opacity and angiogenesis. Similar clinical findings are detected in refractory ocular surface diseases, such as Stevens-Johnson Syndrome (SJS)⁵⁸, graft versus host disease (GVHD)⁵⁹, ocular

cicatricial pemphigoid (OCP)⁶⁰, or Sjögren's syndrome⁶¹, which are all associated with severe DE.

Therapeutic interventions for DE mainly alleviate the symptoms - for example, by using hyaluronic acid-containing eye drops. Recent studies have shown that regulation of T cell activation using drugs such as cyclosporine or ICAM-1 inhibitor represents another potential target for DE treatment^{62,63}. This is related to the fact that DE can be caused by chronic inflammation. However, it is still unclear how chronic inflammation exerts its effects during DE, and the links between SOCs and inflammation in the eye still need to be investigated.

The SASP can act in a paracrine manner to alter the organization and function of neighboring normal cells. Even though secondary senescence was not investigated in our study, we determined that cellular senescence at the ocular surface participated in the pathophysiology of DE and that elimination of senescent cells protected from corneal opacity. The extensive characterization of the ocular SASP could lead to the development of diagnostic tools and treatments based on the presence of SOC and on the use of senolytic agents.

Supplementary Material

Refer to Web version on PubMed Central for supplementary material.

ACKNOWLEDGMENTS

We thank Masahiro Nakamura, Pacome Lecot, Jun-Wei B. Hughes, Chisaka Kuehnemann, Francesco Neri, and Corey Webster for helpful scientific discussion. The work was supported by the National Institutes of Health grants R01 AG009909 and P01 AG017242 (JC), and U01 AG060906 (BS), and partly supported by a Glenn Foundation fellowship (SKP), and by the Japan Society for the Promotion of Science (#201960725), Japan Eye Bank Association, and Alcon Novartis Hida Memorial Award 2017 (KK).

DATA AVAILABILITY STATEMENT

Raw data and complete MS data sets have been uploaded to the Mass Spectrometry Interactive Virtual Environment (MassIVE) repository, developed by the Center for Computational Mass Spectrometry at the University of California San Diego, and can be downloaded using the following link: <ftp://MSV000090204@massive.ucsd.edu> (MassIVE ID number: MSV000090204; ProteomeXchange ID: PXD036253). Raw data set for RNA-seq were deposited in GEO (accession number: GSE232508).

ABBREVIATIONS

ACTB	beta actin
AGC	automatic gain control
AR	androgen receptor
CAPS	calcyphosin
CCL	c-c motif chemokine ligand

CoC	corneal epithelial cells
CM	conditioned medium
CXCL	c-x-c motif chemokine ligand
DAPI	4',6-diamidino-2-phenylindole
DE	dry eye
DIA	data-independent acquisition
EdU	5-ethynyl-2'-deoxyuridine
ER	estrogen receptor
GCV	ganciclovir
GDF15	growth differentiation factor 15
GO	gene ontology
GVHD	graft versus host disease
HMGB1	high mobility group box 1
HSV-TK	herpes simplex virus thymidine kinase
ICAM1	intercellular adhesion molecule-1
IL	interleukin
IR	ionizing radiation
LGE	lacrimal gland excision
LMNB1	lamin B1
LTBP3	latent transforming growth factor beta binding protein 3
LUM	lumican
MAPK	mitogen-activated protein kinases
MMP	matrix metalloproteinase
MS	mass spectrometry
NS	non-senescent cells
OCP	ocular cicatricial pemphigoid
PLS-DA	partial least squares discriminant analysis
qRT-PCR	quantitative reverse transcription polymerase chain reaction
RFP	red fluorescent protein

rLUC	Renilla luciferase
SA-β-Gal	senescence-associated β -galactosidase
SASP	senescence-associated secretory phenotype
SERPIN	serine proteinase inhibitor
SOC	senescent ocular cell
TEAB	triethylammonium bicarbonate
TEER	transepithelial electrical resistance
TNF	tumor necrosis factor
VEGF	vascular endothelial growth factor

REFERENCES

1. Kitazawa K, Inomata T, Shih K, Hughes JB, Bozza N, Tomioka Y, Numa K, Yokoi N, Campisi J, Dana R, Sotozono C. Impact of aging on the pathophysiology of dry eye disease: A systematic review and meta-analysis. *Ocul Surf.* 2022; 25: 108–118. [PubMed: 35753664]
2. Giebel J, Woenckhaus C, Fabian M, Tost F. Age-related differential expression of apoptosis-related genes in conjunctival epithelial cells. *Acta Ophthalmol Scand.* 2005; 83(4):471–476. [PubMed: 16029273]
3. Nien CJ, Massei S, Lin G, Nabavi C, Tao J, Brown DJ, Paugh JR, Jester JV. Effects of age and dysfunction on human meibomian glands. *Arch Ophthalmol.* 2011; 129(4): 462–469. [PubMed: 21482872]
4. Parfitt GJ, Xie Y, Geyfman M, Brown DJ, Jester JV. Absence of ductal hyper-keratinization in mouse age-related meibomian gland dysfunction (ARMGD). *Aging (Albany NY).* 2013; 5(11): 825–834. [PubMed: 24259272]
5. Parfitt GJ, Brown DJ, Jester JV. Transcriptome analysis of aging mouse meibomian glands. *Mol Vis.* 2016; 22: 518–527. [PubMed: 27279727]
6. Yoon CH, Ryu JS, Hwang HS, Kim MK. Comparative Analysis of Age-Related Changes in Lacrimal Glands and Meibomian Glands of a C57BL/6 Male Mouse Model. *Int J Mol Sci.* 2020; 21(11): 4169. [PubMed: 32545199]
7. Lopez-Otin C, Blasco MA, Partridge L, Serrano M, Kroemer G. The hallmarks of aging. *Cell.* 2013; 153(6): 1194–1217. [PubMed: 23746838]
8. Furman D, Campisi J, Verdin E, Carrera-Bastos P, Targ S, Franceschi C, Ferrucci L, Gilroy DW, Fasano A, Miller GW, Miller AH, Mantovani A, Weyand CM, Barzilai N, Goronzy JJ, Rando TA, Effros RB, Lucia A, Kleinstreuer N, Slavich GM. Chronic inflammation in the etiology of disease across the life span. *Nat Med.* 2019; 25(12): 1822–1832. [PubMed: 31806905]
9. Herranz N, Gil J. Mechanisms and functions of cellular senescence. *J Clin Invest.* 2018; 128(4): 1238–1246. [PubMed: 29608137]
10. Hayflick L, Moorhead PS. The serial cultivation of human diploid cell strains. *Exp Cell Res.* 1961; 25: 585–621. [PubMed: 13905658]
11. Campisi J. Senescent cells, tumor suppression, and organismal aging: good citizens, bad neighbors. *Cell.* 2005; 120(4): 513–522. [PubMed: 15734683]
12. Coppe JP, Patil CK, Rodier F, Sun Y, Munoz DP, Goldstein J, Nelson PS, Desprez PY, Campisi J. Senescence-associated secretory phenotypes reveal cell-nonautonomous functions of oncogenic RAS and the p53 tumor suppressor. *PLoS Biol.* 2008; 6(12): 2853–2868. 2592359. [PubMed: 19053174]
13. Basisty N, Kale A, Jeon OH, Kuehnemann C, Payne T, Rao C, Holtz A, Shah S, Sharma V, Ferrucci L, Campisi J, Schilling B. A proteomic atlas of senescence-associated secretomes for

aging biomarker development. *PLoS Biol.* 2020; 18(1): e3000599. following competing interests: JC is a founder and shareholder of Unity Biotechnology, which develops senolytic drugs. All other authors have declared no competing interests. [PubMed: 31945054]

14. Jeon OH, Kim C, Laberge RM, Demaria M, Rathod S, Vasserot AP, Chung JW, Kim DH, Poon Y, David N, Baker DJ, van Deursen JM, Campisi J, Elisseeff JH. Local clearance of senescent cells attenuates the development of post-traumatic osteoarthritis and creates a pro-regenerative environment. *Nat Med.* 2017; 23(6): 775–781. 5785239. [PubMed: 28436958]
15. Chang J, Wang Y, Shao L, Laberge RM, Demaria M, Campisi J, Janakiraman K, Sharpless NE, Ding S, Feng W, Luo Y, Wang X, Aykin-Burns N, Krager K, Ponnappan U, Hauer-Jensen M, Meng A, Zhou D. Clearance of senescent cells by ABT263 rejuvenates aged hematopoietic stem cells in mice. *Nat Med.* 2016; 22(1): 78–83. [PubMed: 26657143]
16. Childs BG, Baker DJ, Wijshake T, Conover CA, Campisi J, van Deursen JM. Senescent intimal foam cells are deleterious at all stages of atherosclerosis. *Science.* 2016; 354(6311): 472–477. [PubMed: 27789842]
17. De Paiva CS, Villarreal AL, Corrales RM, Rahman HT, Chang VY, Farley WJ, Stern ME, Niederkorn JY, Li DQ, Pflugfelder SC. Dry eye-induced conjunctival epithelial squamous metaplasia is modulated by interferon-gamma. *Invest Ophthalmol Vis Sci.* 2007; 48(6): 2553–2560. [PubMed: 17525184]
18. Bian F, Xiao Y, Barbosa FL, de Souza RG, Hernandez H, Yu Z, Pflugfelder SC, de Paiva CS. Age-associated antigen-presenting cell alterations promote dry-eye inducing Th1 cells. *Mucosal Immunol.* 2019; 12(4): 897–908. [PubMed: 30696983]
19. Kitazawa K, Hikichi T, Nakamura T, Mitsunaga K, Tanaka A, Nakamura M, Yamakawa T, Furukawa S, Takasaka M, Goshima N, Watanabe A, Okita K, Kawasaki S, Ueno M, Kinoshita S, Masui S. OVOL2 Maintains the Transcriptional Program of Human Corneal Epithelium by Suppressing Epithelial-to-Mesenchymal Transition. *Cell Rep.* 2016; 15(6): 1359–1368. [PubMed: 27134177]
20. Nakamura T, Yokoo S, Bentley AJ, Nagata M, Fullwood NJ, Inatomi T, Sotozono C, Yamagami S, Kinoshita S. Development of functional human oral mucosal epithelial stem/progenitor cell sheets using a feeder-free and serum-free culture system for ocular surface reconstruction. *Sci Rep.* 2016; 6: 37173. 5107917. [PubMed: 27841343]
21. Demaria M, O’Leary MN, Chang J, Shao L, Liu S, Alimirah F, Koenig K, Le C, Mitin N, Deal AM, Alston S, Academia EC, Kilmarx S, Valdovinos A, Wang B, de Bruin A, Kennedy BK, Melov S, Zhou D, Sharpless NE, Muss H, Campisi J. Cellular Senescence Promotes Adverse Effects of Chemotherapy and Cancer Relapse. *Cancer Discov.* 2017; 7(2): 165–176. [PubMed: 27979832]
22. Chang BD, Swift ME, Shen M, Fang J, Broude EV, Roninson IB. Molecular determinants of terminal growth arrest induced in tumor cells by a chemotherapeutic agent. *Proc Natl Acad Sci U S A.* 2002; 99(1): 389–394. [PubMed: 11752408]
23. Alimirah F, Pulido T, Valdovinos A, Alptekin S, Chang E, Jones E, Diaz DA, Flores J, Velarde MC, Demaria M, Davalos AR, Wiley CD, Limbad C, Desprez PY, Campisi J. Cellular Senescence Promotes Skin Carcinogenesis through p38MAPK and p44/42MAPK Signaling. *Cancer Res.* 2020; 80(17): 3606–3619. [PubMed: 32641409]
24. Kitazawa K, Hikichi T, Nakamura T, Sotozono C, Kinoshita S, Masui S. PAX6 regulates human corneal epithelium cell identity. *Exp Eye Res.* 2017; 154: 30–38. [PubMed: 27818314]
25. Kitazawa K, Kawasaki S, Shinomiya K, Aoi K, Matsuda A, Funaki T, Yamasaki K, Nakatsukasa M, Ebihara N, Murakami A, Hamuro J, Kinoshita S. Establishment of a human corneal epithelial cell line lacking the functional TACSTD2 gene as an in vitro model for gelatinous drop-like dystrophy. *Invest Ophthalmol Vis Sci.* 2013; 54(8): 5701–5711. [PubMed: 23868985]
26. Martin MP. Cutadapt Removes Adapter Sequences from High-Throughput Sequencing Reads. *EMBnet Journal.* 2011; 17: 10–12.
27. Kim D, Langmead B, Salzberg SL. HISAT: a fast spliced aligner with low memory requirements. *Nat Methods.* 2015; 12(4): 357–360. [PubMed: 25751142]
28. Li H, Handsaker B, Wysoker A, Fennell T, Ruan J, Homer N, Marth G, Abecasis G, Durbin R, Genome Project Data Processing S. The Sequence Alignment/Map format and SAMtools. *Bioinformatics.* 2009; 25(16): 2078–2079. 2723002. [PubMed: 19505943]

29. Liao Y, Smyth GK, Shi W. featureCounts: an efficient general purpose program for assigning sequence reads to genomic features. *Bioinformatics*. 2014; 30(7): 923–930. [PubMed: 24227677]
30. Love MI, Huber W, Anders S. Moderated estimation of fold change and dispersion for RNA-seq data with DESeq2. *Genome Biol*. 2014; 15(12): 550. [PubMed: 25516281]
31. Escher C, Reiter L, MacLean B, Ossola R, Herzog F, Chilton J, MacCoss MJ, Rinner O. Using iRT, a normalized retention time for more targeted measurement of peptides. *Proteomics*. 2012; 12(8): 1111–1121. [PubMed: 22577012]
32. Gillet LC, Navarro P, Tate S, Rost H, Selevsek N, Reiter L, Bonner R, Aebersold R. Targeted data extraction of the MS/MS spectra generated by data-independent acquisition: a new concept for consistent and accurate proteome analysis. *Mol Cell Proteomics*. 2012; 11(6): O111 016717.
33. Bruderer R, Bernhardt OM, Gandhi T, Xuan Y, Sondermann J, Schmidt M, Gomez-Varela D, Reiter L. Optimization of Experimental Parameters in Data-Independent Mass Spectrometry Significantly Increases Depth and Reproducibility of Results. *Mol Cell Proteomics*. 2017; 16(12): 2296–2309. [PubMed: 29070702]
34. Collins BC, Hunter CL, Liu Y, Schilling B, Rosenberger G, Bader SL, Chan DW, Gibson BW, Gingras AC, Held JM, Hirayama-Kurogi M, Hou G, Krisp C, Larsen B, Lin L, Liu S, Molloy MP, Moritz RL, Ohtsuki S, Schlapbach R, Selevsek N, Thomas SN, Tzeng SC, Zhang H, Aebersold R. Multi-laboratory assessment of reproducibility, qualitative and quantitative performance of SWATH-mass spectrometry. *Nat Commun*. 2017; 8(1): 291. [PubMed: 28827567]
35. Burger T. Gentle Introduction to the Statistical Foundations of False Discovery Rate in Quantitative Proteomics. *J Proteome Res*. 2018; 17(1): 12–22. [PubMed: 29067805]
36. Demaria M, Ohtani N, Youssef SA, Rodier F, Toussaint W, Mitchell JR, Laberge RM, Vijg J, Van Steeg H, Dolle ME, Hoeijmakers JH, de Bruin A, Hara E, Campisi J. An essential role for senescent cells in optimal wound healing through secretion of PDGF-AA. *Dev Cell*. 2014; 31(6): 722–733. [PubMed: 25499914]
37. Baker DJ, Wijshake T, Tchkonia T, LeBrasseur NK, Childs BG, van de Sluis B, Kirkland JL, van Deursen JM. Clearance of p16Ink4a-positive senescent cells delays ageing-associated disorders. *Nature*. 2011; 479(7372): 232–236. [PubMed: 22048312]
38. Baker DJ, Childs BG, Durik M, Wijers ME, Sieben CJ, Zhong J, Saltness RA, Jeganathan KB, Verzosa GC, Pezeshki A, Khazaie K, Miller JD, van Deursen JM. Naturally occurring p16(Ink4a)-positive cells shorten healthy lifespan. *Nature*. 2016; 530(7589): 184–189. [PubMed: 26840489]
39. Shinomiya K, Ueta M, Kinoshita S. A new dry eye mouse model produced by exorbital and intraorbital lacrimal gland excision. *Sci Rep*. 2018; 8(1): 1483. [PubMed: 29367638]
40. Coppe JP, Desprez PY, Krtolica A, Campisi J. The senescence-associated secretory phenotype: the dark side of tumor suppression. *Annu Rev Pathol*. 2010; 5: 99–118. [PubMed: 20078217]
41. Freund A, Laberge RM, Demaria M, Campisi J. Lamin B1 loss is a senescence-associated biomarker. *Mol Biol Cell*. 2012; 23(11): 2066–2075. [PubMed: 22496421]
42. Parrinello S, Coppe JP, Krtolica A, Campisi J. Stromal-epithelial interactions in aging and cancer: senescent fibroblasts alter epithelial cell differentiation. *J Cell Sci*. 2005; 118(Pt 3): 485–496. [PubMed: 15657080]
43. Chang SW, Hu FR. Changes in corneal autofluorescence and corneal epithelial barrier function with aging. *Cornea*. 1993; 12(6): 493–499. [PubMed: 8261780]
44. Campisi J, d'Adda di Fagagna F. Cellular senescence: when bad things happen to good cells. *Nat Rev Mol Cell Biol*. 2007; 8(9): 729–740. [PubMed: 17667954]
45. Li ZY, Chen ZL, Zhang T, Wei C, Shi WY. TGF-beta and NF-kappaB signaling pathway crosstalk potentiates corneal epithelial senescence through an RNA stress response. *Aging (Albany NY)*. 2016; 8(10): 2337–2354. [PubMed: 27713146]
46. Martin N, Bernard D. Calcium signaling and cellular senescence. *Cell Calcium*. 2018; 70: 16–23. [PubMed: 28410770]
47. Shikama Y, Kurosawa M, Furukawa M, Ishimaru N, Matsushita K. Involvement of adiponectin in age-related increases in tear production in mice. *Aging (Albany NY)*. 2019; 11(19): 8329–8346. [PubMed: 31596727]

48. McClellan AJ, Volpe EA, Zhang X, Darlington GJ, Li DQ, Pflugfelder SC, de Paiva CS. Ocular surface disease and dacryoadenitis in aging C57BL/6 mice. *Am J Pathol.* 2014; 184(3): 631–643. [PubMed: 24389165]
49. Stevenson W, Chen Y, Lee SM, Lee HS, Hua J, Dohlman T, Shiang T, Dana R. Extraorbital lacrimal gland excision: a reproducible model of severe aqueous tear-deficient dry eye disease. *Cornea.* 2014; 33(12): 1336–1341. [PubMed: 25255136]
50. Guzman M, Keitelman I, Sabbione F, Trevani AS, Giordano MN, Galletti JG. Mucosal tolerance disruption favors disease progression in an extraorbital lacrimal gland excision model of murine dry eye. *Exp Eye Res.* 2016; 151: 19–22. [PubMed: 27443502]
51. Kim CS, Jo K, Lee IS, Kim J. Topical Application of Apricot Kernel Extract Improves Dry Eye Symptoms in a Unilateral Exorbital Lacrimal Gland Excision Mouse. *Nutrients.* 2016; 8(11).
52. Mecum NE, Cyr D, Malon J, Demers D, Cao L, Meng ID. Evaluation of Corneal Damage After Lacrimal Gland Excision in Male and Female Mice. *Invest Ophthalmol Vis Sci.* 2019; 60(10): 3264–3274. [PubMed: 31369671]
53. Ovadya Y, Landsberger T, Leins H, Vadai E, Gal H, Biran A, Yosef R, Sagiv A, Agrawal A, Shapira A, Windheim J, Tsoory M, Schirmbeck R, Amit I, Geiger H, Krizhanovsky V. Impaired immune surveillance accelerates accumulation of senescent cells and aging. *Nat Commun.* 2018; 9(1): 5435. [PubMed: 30575733]
54. Ressler S, Bartkova J, Niederegger H, Bartek J, Scharffetter-Kochanek K, Jansen-Durr P, Wlaschek M. p16INK4A is a robust in vivo biomarker of cellular aging in human skin. *Aging Cell.* 2006; 5(5): 379–389. [PubMed: 16911562]
55. Azcarate PM, Venincasa VD, Feuer W, Stanczyk F, Schally AV, Galor A. Androgen deficiency and dry eye syndrome in the aging male. *Invest Ophthalmol Vis Sci.* 2014; 55(8): 5046–5053. [PubMed: 24994872]
56. Campisi J, Robert L. Cell senescence: role in aging and age-related diseases. *Interdiscip Top Gerontol.* 2014; 39: 45–61. [PubMed: 24862014]
57. Tomioka Y, Kitazawa K, Numa K, Yokoi N, Sotozono C. UVA-Induced Cellular Senescence in Human Conjunctival Epithelium. *Invest Ophthalmol Vis Sci.* 2023; 64(8): 2028.
58. Sotozono C, Ueta M, Kinoshita S. Japan: Diagnosis and Management of Stevens-Johnson Syndrome/Toxic Epidermal Necrolysis With Severe Ocular Complications. *Front Med (Lausanne).* 2021; 8: 657327. [PubMed: 34395463]
59. Wolff D, Radojic V, Lafyatis R, Cinar R, Rosenstein RK, Cowen EW, Cheng GS, Sheshadri A, Bergeron A, Williams KM, Todd JL, Teshima T, Cuvelier GDE, Holler E, McCurdy SR, Jenq RR, Hanash AM, Jacobsohn D, Santomaso BD, Jain S, Ogawa Y, Steven P, Luo ZK, Dietrich-Ntoukas T, Saban D, Bilic E, Penack O, Griffith LM, Cowden M, Martin PJ, Greinix HT, Sarantopoulos S, Socie G, Blazar BR, Pidala J, Kitko CL, Couriel DR, Cutler C, Schultz KR, Pavletic SZ, Lee SJ, Paczesny S. National Institutes of Health Consensus Development Project on Criteria for Clinical Trials in Chronic Graft-versus-Host Disease: IV. The 2020 Highly morbid forms report. *Transplant Cell Ther.* 2021; 27(10): 817–835. [PubMed: 34217703]
60. Branisteanu DC, Stoleriu G, Branisteanu DE, Boda D, Branisteanu CI, Maranduca MA, Moraru A, Stanca HT, Zemba M, Balta F. Ocular cicatricial pemphigoid (Review). *Exp Ther Med.* 2020; 20(4): 3379–3382. [PubMed: 32905166]
61. Donthineni PR, Doctor MB, Shanbhag S, Kate A, Galor A, Djalilian AR, Singh S, Basu S. Aqueous-deficient dry eye disease: Preferred practice pattern guidelines on clinical approach, diagnosis, and management. *Indian J Ophthalmol.* 2023; 71(4): 1332–1347. [PubMed: 37026265]
62. Keating GM. Lifitegrast Ophthalmic Solution 5%: A Review in Dry Eye Disease. *Drugs.* 2017; 77(2): 201–208. [PubMed: 28058622]
63. Baiza-Duran L, Medrano-Palafox J, Hernandez-Quintela E, Lozano-Alcazar J, Alaniz-de la OJ. A comparative clinical trial of the efficacy of two different aqueous solutions of cyclosporine for the treatment of moderate-to-severe dry eye syndrome. *Br J Ophthalmol.* 2010; 94(10): 1312–1315. [PubMed: 20679084]

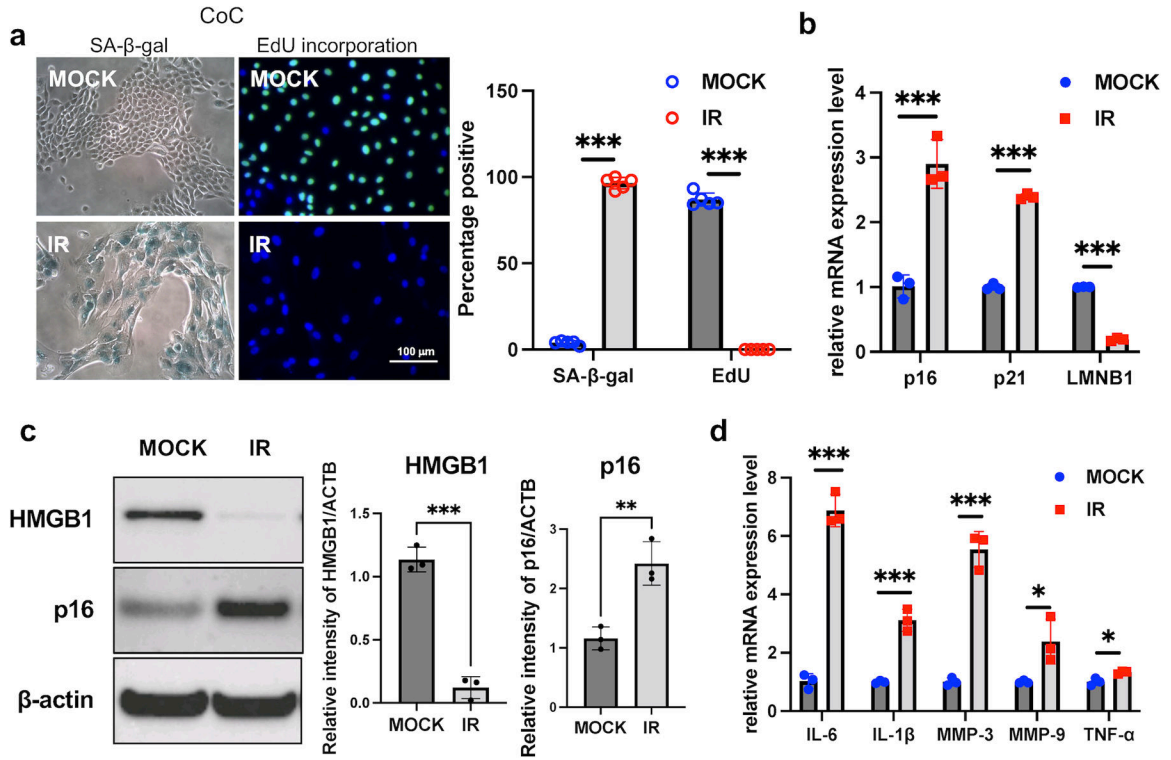


Figure 1. Characteristics of human SOC.

a, SA-β-Gal staining and EdU labeling of corneal epithelial cells upon IR-induced senescence. Corneal epithelial cells were treated with 10 Gy IR (or mock as control) and cultured for 10 days. SA-β-Gal expression and EdU labeling were performed 10 days after treatment. Representative images are shown (left) and results are plotted as mean % of positive cells from five independent experiments (right). b, Using real-time PCR, RNA expression analysis of *p16*, *p21* and *LMNB1* in control cells and IR-treated cells from human cornea. c, Protein expression analysis and quantification of p16 and HMGB1 in control cells and IR-treated cells from human cornea using western blotting. d, Using real-time PCR, RNA expression analysis of SASP factors (*IL-6*, *IL-1β*, *MMP-3*, *MMP-9*, *TNF-α*) in control cells and IR-treated cells from cornea. Results were plotted as mean and standard deviation from three independent experiments. Gene expression was normalized to the housekeeping gene *ACTB*. * = $p < 0.05$; ** = $p < 0.01$; *** = $p < 0.001$.

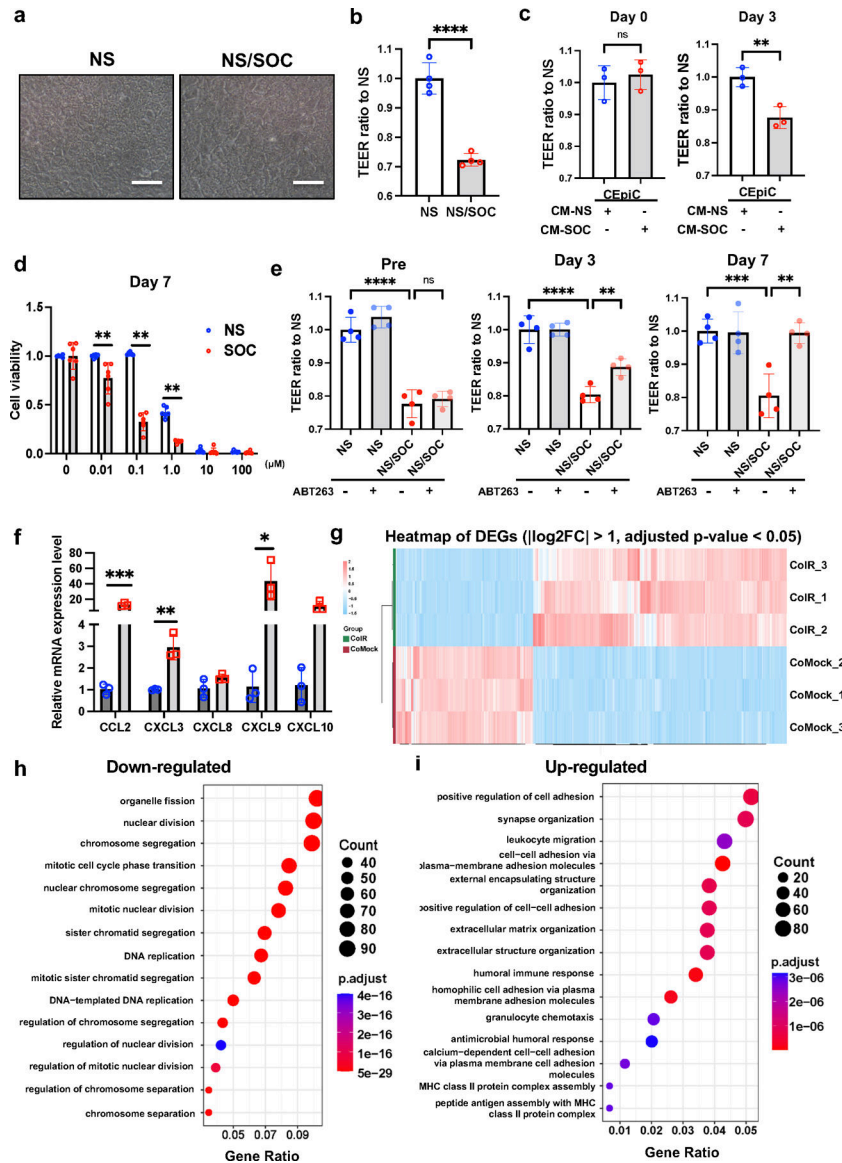


Figure 2. Measurement of TEER as an epithelial barrier in human corneal epithelial cells and effects of a senolytic agent.

a, Senescent human corneal epithelial cells (SOC, IR-treated cells) were seeded together with non-senescent human corneal epithelial cells (NS, mock-treated cells) at a ratio of 3/1 in the upper wells of transwell plates. b, The TEER of NS alone or SOC together with NS was measured. c, Human corneal epithelial cells were seeded, and, after reaching cell confluency, the CM from NS or SOC were added, and the TEER measured until day 3 post CM treatment. d, Timeline of cell viability assay upon ABT263 treatment. Cells were treated with IR or mock, and then treated with ABT263 at 0, 0.01, 0.1, 1.0, 10, 100 μ M. Cell viability was analyzed at day 7. Results were plotted as mean and standard deviation from six independent experiments. The average value at 0 μ M for each group was set at 100% cell viability. e, SOCs were seeded with NS at a ratio of 3/1 in the upper wells of transwell plates, treated with the senolytic agent ABT263 at 0.1 μ M, and their TEER measured over time. Results were plotted as mean and standard deviation from four independent

experiments. f, Using real-time PCR, RNA expression analysis of chemokine-related genes (*CCL2*, *CXCL3*, *CXCL8*, *CXCL9*, *CXCL10*) in control cells and IR-treated cells from human cornea. g, Heat map of differential gene expressions comparing NS and SOCs. h, Pathway and network analysis of gene expressions that are significantly decreased in SOCs compared to NS. i, Pathway and network analysis of gene expressions that are significantly increased in SOCs compared to NS. Gene expression was normalized to the housekeeping gene *ACTB*. * = $p < 0.05$; ** = $p < 0.01$; *** = $p < 0.001$.

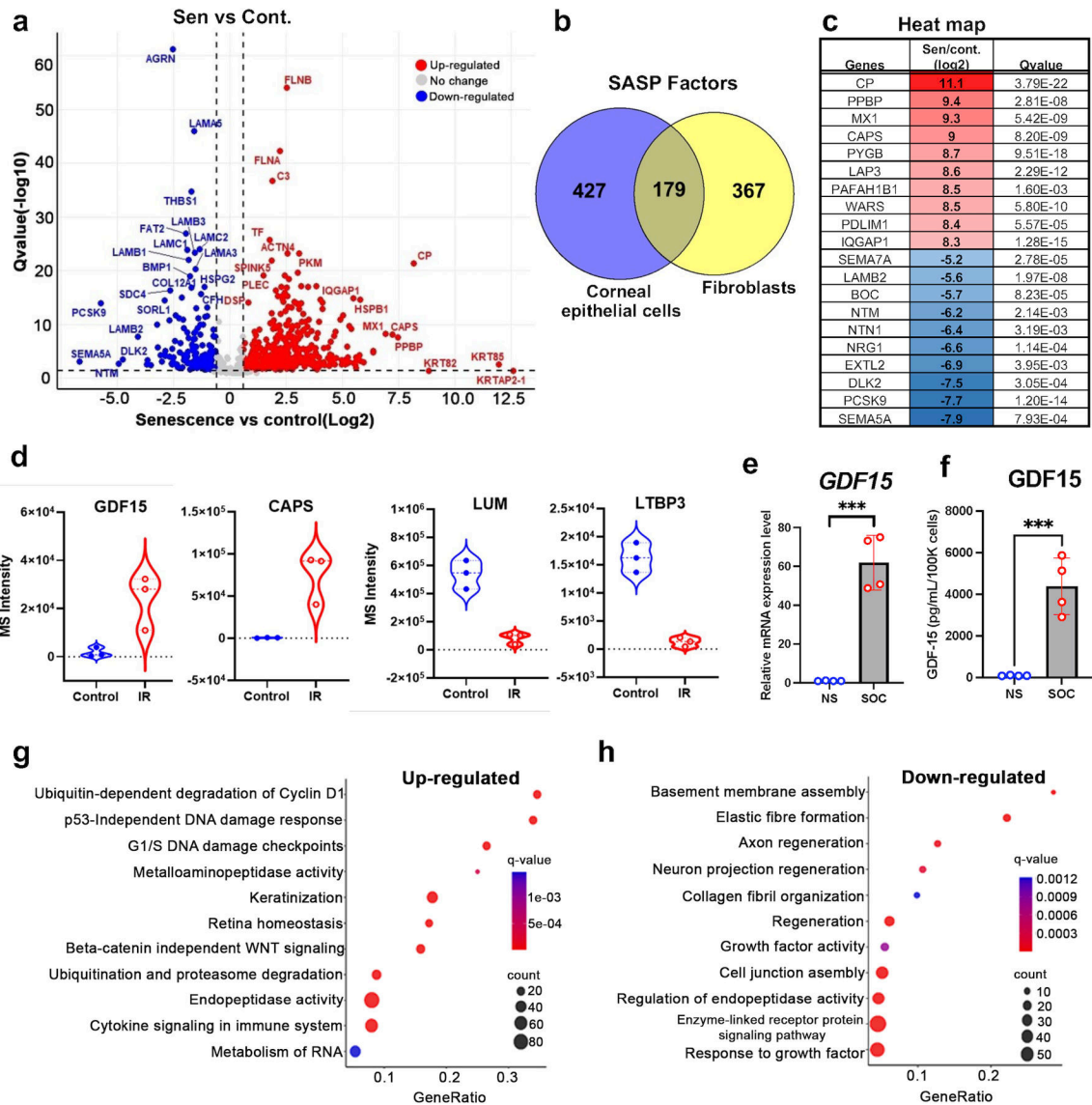


Figure 3: Unbiased quantitative proteome profile of human corneal SASP.

a, CM from IR-induced senescent human corneal epithelial cells (SOC) (n = 3) and non-senescent human corneal epithelial cells (control) (n = 3) were fractionated using HPLC and analyzed using mass spectrometry. Volcano plot showing Q values (–log10) vs. fold change of (log2) SOC and control corneal epithelial cells. Blue, downregulated; red, up-regulated; and black, no significant change (2 unique peptides, fold change 1.5, q-value 0.05). b, Venn diagram showing unique and integral significantly altered SASP proteins (2 unique peptides, fold change 1.5, q-value 0.05) in IR-induced corneal epithelial cells and human lung fibroblast cells (IMR-90). c, Table showing top 10 up- or down-regulated cornea SASP proteins. d, Violin plot showing the individual differential expression of GDF-15, CAPS, LUM and LTBP3 comparing quiescent controls and SOCs. Results are shown as biological replicates and mean ± SD, and paired t-test showed significant differences between groups. e, Using real-time PCR, RNA expression analysis of *GDF15* in SOCs compared to NS. Gene expression was normalized to the housekeeping gene *ACTB*. f, ELISA analysis of GDF15

protein expression in corneal SASP. g, Pathway and network analysis of secreted proteins that are significantly increased in corneal SASP. h, Pathway and network analysis of secreted proteins that are significantly decreased in corneal SASP. *** = $p < 0.001$.

Author Manuscript

Author Manuscript

Author Manuscript

Author Manuscript

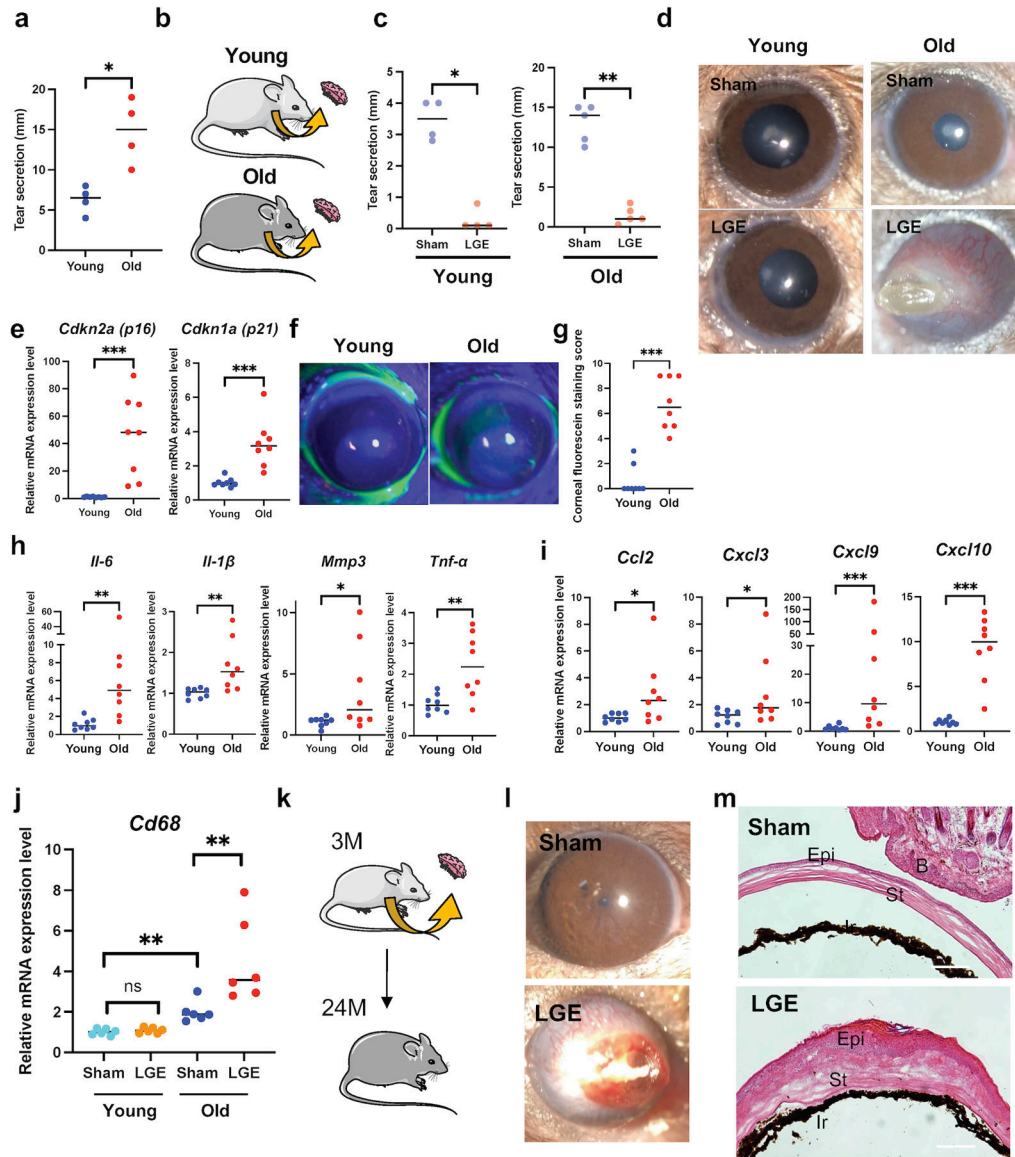


Figure 4. Changes at the ocular surface after LGE in young and old mice.

a, Tear secretion was measured using the cotton thread with phenol red in eyes of young mice (n = 4) and old mice (n = 4). b, LGE was performed on the right side and sham surgery on the left side of young mice (4 months of age) and old mice (24 months of age). c, Tear secretion was measured using the cotton thread with phenol red in eyes of young mice post sham control (n = 4) or after LGE (n = 4) and old mice post sham control (n = 5) or after LGE (n = 5). d, Representative slit-lamp images of ocular surfaces in young or old control mice and in young or old mice one month after LGE surgery. e, Using real-time PCR, RNA expression analysis of *p16* and *p21* in cornea of young mice (4 months of age) and old mice (24 months of age). f, Representative corneal fluorescein staining images in young and old mice. g, Corneal epithelial damage was assessed with fluorescein staining. A corneal fluorescein staining score was assigned with 1 to 3 at each 1/3 area of the cornea (upper, intermediate, and lower), in young mice (4 months of age) and old mice (24 months

of age). h, Using real-time PCR, RNA expression analysis of SASP-related genes including *Il-6*, *Il-1 β* , *Mmp3*, and *Tnf- α* in cornea from young and old mice. i, Using real-time PCR, RNA expression analysis of various chemokine-related genes including *Ccl2*, *Cxcl3*, *Cxcl9* and *Cxcl10* in cornea from young and old mice. j, Using real-time PCR, RNA expression analysis of *Cd68* and *F4/80* in cornea from young and old mice post sham control (n = 6) or after LGE (n = 6). k, Old mice (24 months of age) post sham or LGE performed at young age (3 months) were used. l, Representative slit-lamp images of ocular surfaces and corneal fluorescein staining images in old mice (24 months of age) with or without LGE surgery. m, Representative HE images of ocular surfaces. Ocular features post sham control or after LGE include cornea opacity, angiogenesis and keratinization. Gene expression was normalized to the housekeeping gene *Actb*. * = $p < 0.05$; ** = $p < 0.01$; *** = $p < 0.001$.

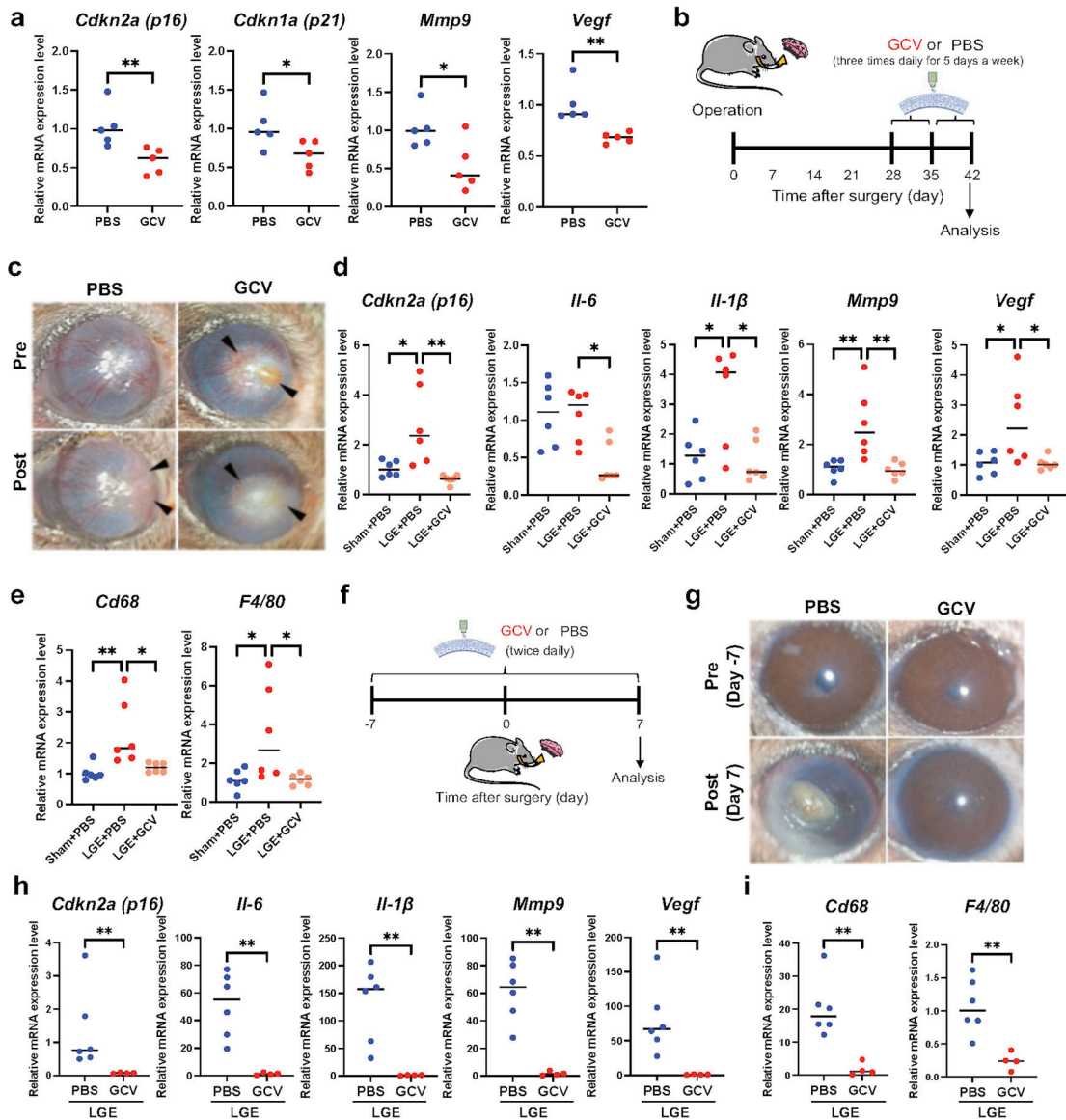


Figure 5. Effects of topical GCV at the ocular surface of old p16-3MR mice post LGE.

a, Using real-time PCR, RNA expression analysis of *p16*, *p21*, *Mmp9*, and *Vegf* in the cornea of old p16-3MR mice (24 months of age) treated with GCV (n = 5) or PBS (n = 5) (used as controls). Both topical GCV and PBS were administered 3 times daily for 5 days for two cycles with a 2-day interval between the cycles. b, Timeline of treated old p16-3MR mice (24 months of age) after LGE. c, Slit-lamp images of the ocular surface of the cornea of old p16-3MR mice treated with GCV compared to mice treated with PBS (used as controls). Both topical GCV and PBS were administered 3 times daily for 5 days for two cycles with a 2-day interval between the cycles. d, Using real-time PCR, RNA expression analysis of *p16* and SASP factors (*Il-6*, *Il-1β*, *Mmp9*, and *Vegf*) in cornea from old p16-3MR mice after either sham surgery or LGE surgery, and topical PBS (-) or GCV (+) treatment (n = 6 per each group). e, Using real-time PCR, RNA expression analysis of *Cd68* and *F4/80* in cornea from old p16-3MR mice after either sham surgery or LGE

surgery, and topical PBS (-) or GCV (+) treatment (n = 6 per each group). f, Timeline of treated old p16-3MR mice (24 months of age) before LGE. g, Slit-lamp images of the ocular surface of the cornea of old p16-3MR mice treated with GCV compared to mice treated with PBS (used as controls). Both topical GCV and PBS were administered 2 times daily for 14 days. h, Using real-time PCR, RNA expression analysis of *p16* and SASP-related genes (*Il-6*, *Il-1 β* , *Mmp9*, *Vegf*). i, Using real-time PCR, RNA expression analysis of *Cd68* and *F4/80* in cornea from old p16-3MR mice after LGE surgery, and topical PBS (-) (n = 6) or GCV (+) treatment (n = 4). Gene expression was normalized to the housekeeping gene *Actb*. * = $p < 0.05$; ** = $p < 0.01$. *** = $p < 0.001$.